

## Raindrop Size Distributions and Rain Characteristics in California Coastal Rainfall for Periods with and without a Radar Bright Band

BROOKS E. MARTNER

*Cooperative Institute for Research in Environmental Sciences, University of Colorado, and NOAA/Earth System Research Laboratory, Boulder, Colorado*

SANDRA E. YUTER

*Department of Marine, Earth, and Atmospheric Sciences, North Carolina State University at Raleigh, Raleigh, North Carolina*

ALLEN B. WHITE, SERGEY Y. MATROSOV, AND DAVID E. KINGSMILL

*Cooperative Institute for Research in Environmental Sciences, University of Colorado, and NOAA/Earth System Research Laboratory, Boulder, Colorado*

F. MARTIN RALPH

*NOAA/Earth System Research Laboratory, Boulder, Colorado*

(Manuscript received 24 April 2007, in final form 21 September 2007)

### ABSTRACT

Recent studies using vertically pointing S-band profiling radars showed that coastal winter storms in California and Oregon frequently do not display a melting-layer radar bright band and inferred that these nonbrightband (NBB) periods are characterized by raindrop size spectra that differ markedly from those of brightband (BB) periods. Two coastal sites in northern California were revisited in the winter of 2003/04 in this study, which extends the earlier work by augmenting the profiling radar observations with collocated raindrop disdrometers to measure drop size distributions (DSD) at the surface. The disdrometer observations are analyzed for more than 320 h of nonconvective rainfall. The new measurements confirm the earlier inferences that NBB rainfall periods are characterized by greater concentrations of small drops and smaller concentrations of large drops than BB periods. Compared with their BB counterparts, NBB periods had mean values that were 40% smaller for mean-volume diameter, 32% smaller for rain intensity, 87% larger for total drop concentration, and 81% larger (steeper) for slope of the exponential DSDs. The differences are statistically significant. Liquid water contents differ very little, however, for the two rain types. Disdrometer-based relations between radar reflectivity ( $Z$ ) and rainfall intensity ( $R$ ) at the site in the Coast Range Mountains were  $Z = 168R^{1.58}$  for BB periods and  $Z = 44R^{1.91}$  for NBB. The much lower coefficient, which is characteristic of NBB rainfall, is poorly represented by the  $Z$ - $R$  equations most commonly applied to data from the operational network of Weather Surveillance Radar-1988 Doppler (WSR-88D) units, which underestimate rain accumulations by a factor of 2 or more when applied to nonconvective NBB situations. Based on the observed DSDs, it is also concluded that polarimetric scanning radars may have some limited ability to distinguish between regions of BB and NBB rainfall using differential reflectivity. However, differential-phase estimations of rain intensity are not useful for NBB rain, because the drops are too small and nearly spherical. On average, the profiler-measured echo tops were 3.2 km lower in NBB periods than during BB periods, and they extended only about 1 km above the 0°C altitude. The findings are consistent with the concept that precipitation processes during BB periods are dominated by ice processes in deep cloud layers associated with synoptic-scale forcing, whereas the more restrained growth of hydrometeors in NBB periods is primarily the result of orographically forced condensation and coalescence processes in much shallower clouds.

---

*Corresponding author address:* Brooks E. Martner, NOAA/ESRL/PSD-2, 325 Broadway, Boulder, CO 80305.  
E-mail: brooks.martner@noaa.gov

DOI: 10.1175/2007JHM924.1

© 2008 American Meteorological Society

## 1. Introduction

The California Land-falling Jets (CALJET, 1997/98) and Pacific Land-falling Jets (PACJET, 2001–03) experiments studied coastal winter storms in California and Oregon. One facet of the studies used new vertically pointing S-band Doppler radar profilers (S-PROF) in combination with rain gauges to observe precipitation characteristics. White et al. (2003) examined S-PROF data from the strong El Niño winter of 1997/98 for a site near Cazadero, California, about 75 km northwest of San Francisco in the mountains of the Coast Range. They discovered that during nonconvective periods the melting-layer radar bright band, which is characteristic of winter rain in most midlatitude locations, was frequently absent above this site, even in heavy rainfall with radar echoes extending well above the freezing level. Microphysical features of the rain were deduced to be significantly different during these non-brightband (NBB) periods from times when a bright band (BB) was present.

Based on the profiler reflectivity and vertical velocity data, White et al. (2003) concluded that NBB rain contains more small drops and fewer large drops than the BB periods. The significantly different nature of the drop size distribution (DSD) in NBB situations, inferred from the S-PROF data, produces an empirical reflectivity–rainfall ( $Z$ – $R$ ) relation that is very different from the ones most commonly used by the National Weather Service (NWS) with the operational Weather Surveillance Radar-1988 Doppler units (WSR-88Ds) [or Next-Generation Weather Radar (NEXRAD)], which seriously underestimate rain rates and accumulations in these situations.

Neiman et al. (2005) examined synoptic conditions and S-PROF data from additional sites and winters and concluded that NBB rainfall is not limited to the Cazadero (CZD) site or to El Niño winters. Depending on the particular site or year, NBB conditions contributed 18% to 50% of the total winter precipitation accumulation. They showed that NBB rain is generally shallower and more closely linked to upslope boundary layer airflow, while BB rainfall is more commonly associated with less stable air, colder cloud tops (from satellite infrared data) and frontal conditions. Kingsmill et al. (2006) found that NBB situations also occur in California's flat Central Valley, although much less often than in the coastal mountains at CZD.

Each of these earlier studies inferred that the BB/NBB differences signify that markedly different precipitation formation processes are responsible for these two kinds of nonconvective rainfall. Their evidence indicates that BB rain usually results from deep, cold-top

clouds that produce ice crystals, which grow by vapor deposition, aggregation, and riming to become large snowflakes and then large raindrops when they melt. In the NBB cases, however, large snowflakes are absent, and multitudes of water drops grow to lesser sizes by condensation aided by upslope flow and by coalescence of drops in a relatively shallow layer near the terrain. Although the presence of small ice crystals cannot be ruled out, the NBB periods resemble liquid-phase processes in most respects.

## 2. HMT-04 operations in the 2003/04 winter

The earlier studies did not have the benefit of direct measurements of raindrop DSDs at the ground. The present study returned to two of the same northern California locations in winter 2003/04 to further examine rain characteristics. This time, however, in addition to using S-PROF, collocated raindrop disdrometers were employed to directly measure the DSD at the surface. The main objective of this study is to reveal contrasts between NBB and BB size distributions and rain parameters more definitively.

The observations were obtained as part of the National Oceanic and Atmospheric Administration's (NOAA's) Hydrometeorology Test Bed (HMT) project, which is referred to for this winter as HMT-04. Figure 1 shows the locations of observation sites used in this study in Sonoma County, California: one S-PROF–disdrometer–rain gauge site was on the coastline at Bodega Bay (BBY) at 12 m MSL and another was at Cazadero (CZD), approximately 10 km inland at 475 m MSL in the Coast Range, 33 km northwest of BBY. Rainfall at CZD experiences more orographic enhancement than at BBY because of the more abrupt lifting of airflow by the local mountainous topography there. This is evidenced by the fact that winter monthly rain accumulations at CZD typically exceed those at BBY by a factor of 2 to 3, according to rain gauge data from CALJET, PACJET, and HMT from 1998 to 2006.

Using the procedure of White et al. (2003) for S-PROF data, precipitating periods were objectively categorized as BB or NBB. Half-hour integrations of the radar data were used, which represent 30–60 individual vertical beams. Use of the half-hour-long sampling duration decreases measurement uncertainties in the radar and rain gauge data. Convective (CV) periods, in which a bright band might be obscured, were identified by inspecting time–height displays of the S-PROF vertical Doppler velocity and reflectivity data for each half-hour initially designated as NBB. Isolated convective cells were identified in this way, and organized convection associated with narrow cold frontal rain-

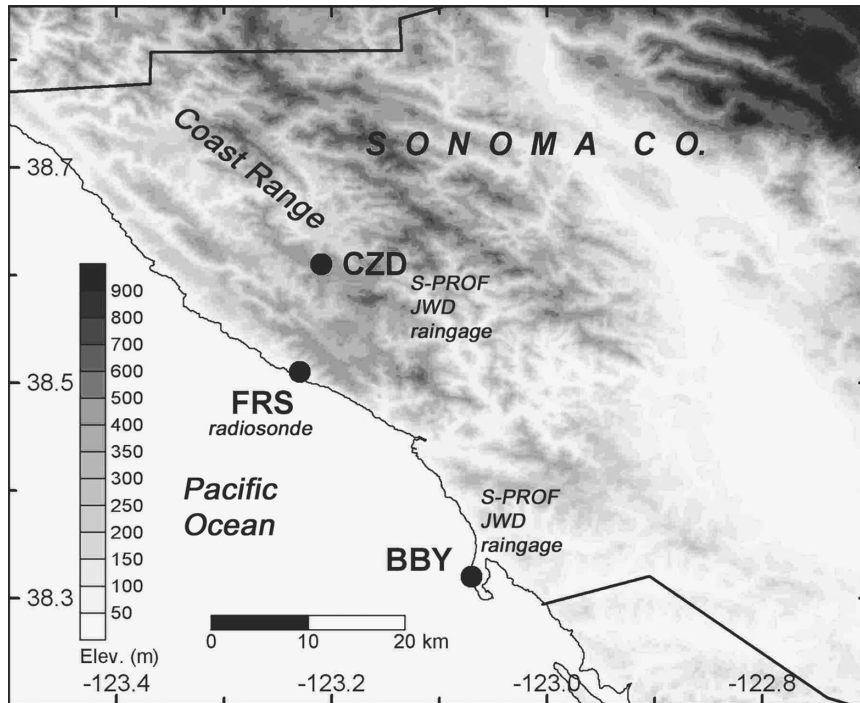


FIG. 1. Map of the Sonoma County area of northern California showing the primary observing sites for this study. Cazadero (CZD) is at 475 m MSL in the Coast Range Mountains; Bodega Bay (BBY) and Fort Ross (FRS) are near sea level on the coastline. The city of San Francisco is approximately 75 km southeast of CZD.

bands was also detected using nearby wind profiler and surface meteorological data in exactly the same manner as in the earlier studies, described by White et al. (2003). The convective periods, which accounted for only 6% of the total number of classified half-hour periods, and 7% of the season's rainfall accumulation, are not examined in this study.

A Joss–Waldvogel disdrometer (JWD) counted and measured the sizes of the raindrops at each profiler site. This instrument senses the momentum of drops impacting on its 50-cm<sup>2</sup> exposed surface (Joss and Waldvogel 1967). Drops were automatically counted in 20 diameter bins ranging from approximately 0.35 to 5.4 mm, and the raw data counts were accumulated and recorded in 1-min intervals. However, for DSD derivations, the raw data were integrated in postprocessing into 10-min samples with data-quality refinements applied, as described in section 3. Rainfall intensity ( $R$ ), radar reflectivity factor ( $Z$ ), and other parameters were computed from the resulting drop size spectra for each sample, which was then tagged with the BB or NBB classification, according to the concurrent 30-min S-PROF data. Daily rain accumulations from the disdrometers agreed with those of the collocated rain gauges within 10% on most days at both sites.

Serial radiosondes were launched at 3-h intervals in several of the storms from Fort Ross (FRS), 11 km south of CZD (Fig. 1). Data from these soundings are used to examine how the S-PROF echoes related to the altitude of the 0°C level. The nearest NEXRAD sites are more than 125 km away from CZD and provide poor low-altitude radar coverage of the study area. The nearest NWS radiosonde site was 110 km away.

### 3. Disdrometer and S-PROF observations in HMT-04

Figure 2 shows an example of an 18-h period of S-PROF and JWD data from the BBY coastline site on 16 February 2004. The storm's time–height history of reflectivity from S-PROF is displayed in the top panel, where a bright band is clearly evident between 2 and 3 km above ground level (AGL) part of the time. The middle panel shows  $R$ ,  $Z$ , and rain accumulation computed from the raw JWD data. In the lower panel, contours of the number of drops counted by the JWD are plotted as a function of time and drop size, where the smallest sizes are at the bottom of the plot. A row of open squares along the top of this panel shows the objective categorization of precipitation as bright band

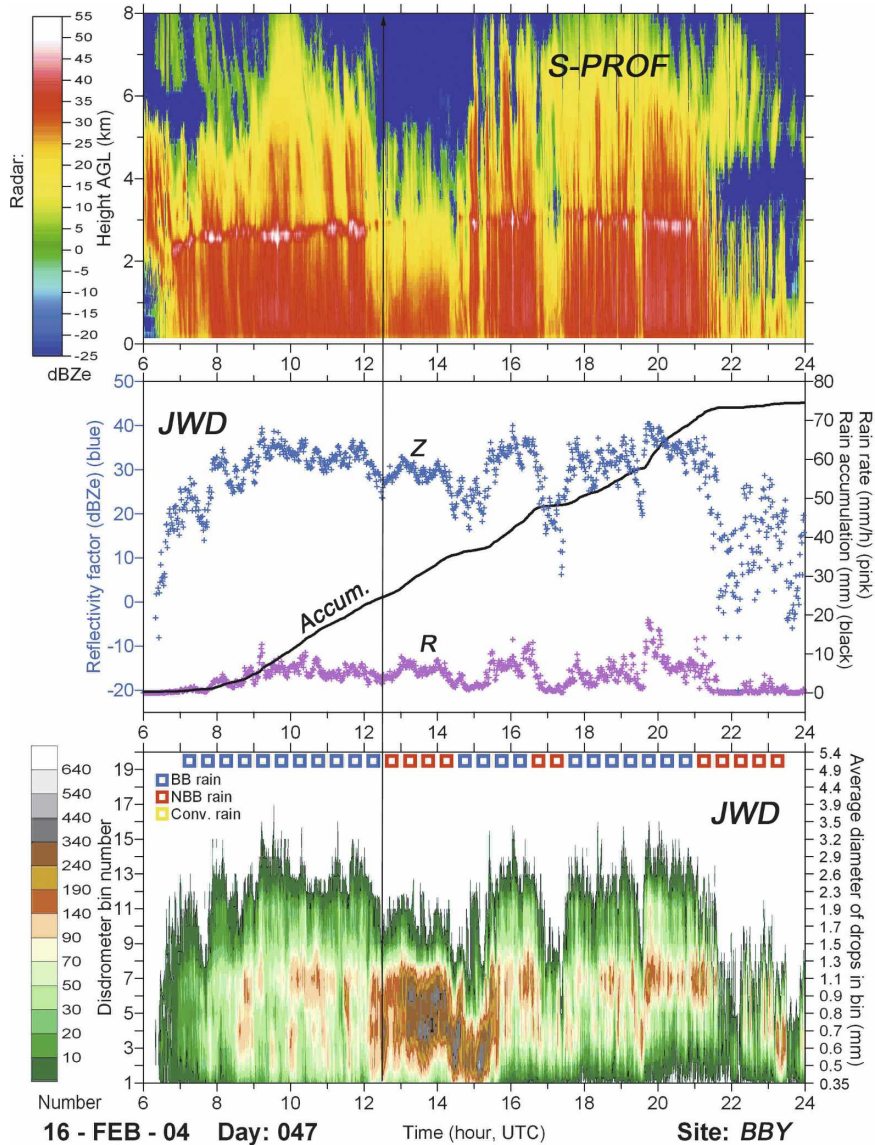


FIG. 2. S-PROF and JWD data from BBY for an 18-h period. (top) A time–height display of reflectivity. (middle) Parameters  $R$ ,  $A$ , and  $Z$  computed from the raw DSD data of the JWD. (bottom) Contoured numbers of drops ( $\text{min}^{-1}$ ) as a function of time and  $D$ . Open squares indicate objective classification of half hours as (blue) BB or (red) NBB rain.

(blue = BB) or non–bright band (red = NBB) according to the S-PROF data for each half hour that the rain gauge had accumulations of at least 0.5 mm.

BB–NBB transitions in this storm are denoted by sequential changes of the blue and red squares in Fig. 2, and associated changes are apparent in the displayed parameters as well. Note the transition at 1230 UTC (vertical line), for example. Although the rainfall intensity remained fairly steady, reflectivity decreased, the echo top lowered sharply (but was still generally above the freezing level), the larger drops disappeared, and there was a very marked increase in the number of

smaller drops, as the category changed from BB to a 2-h period of NBB rainfall.

Figure 3 presents a full-winter statistical summary of the S-PROF Doppler moments data for HMT-04 at CZD, in terms of contoured frequency-by-altitude diagrams (CFAD; Yuter and Houze 1995). These were produced using the same procedures described by White et al. (2003) and by Neiman et al. (2005). In HMT-04, however, an apparent shift of the S-PROF calibration was found by comparing the low-altitude (210 m AGL) S-PROF reflectivity data with those of the collocated disdrometer, using half-hour averaging

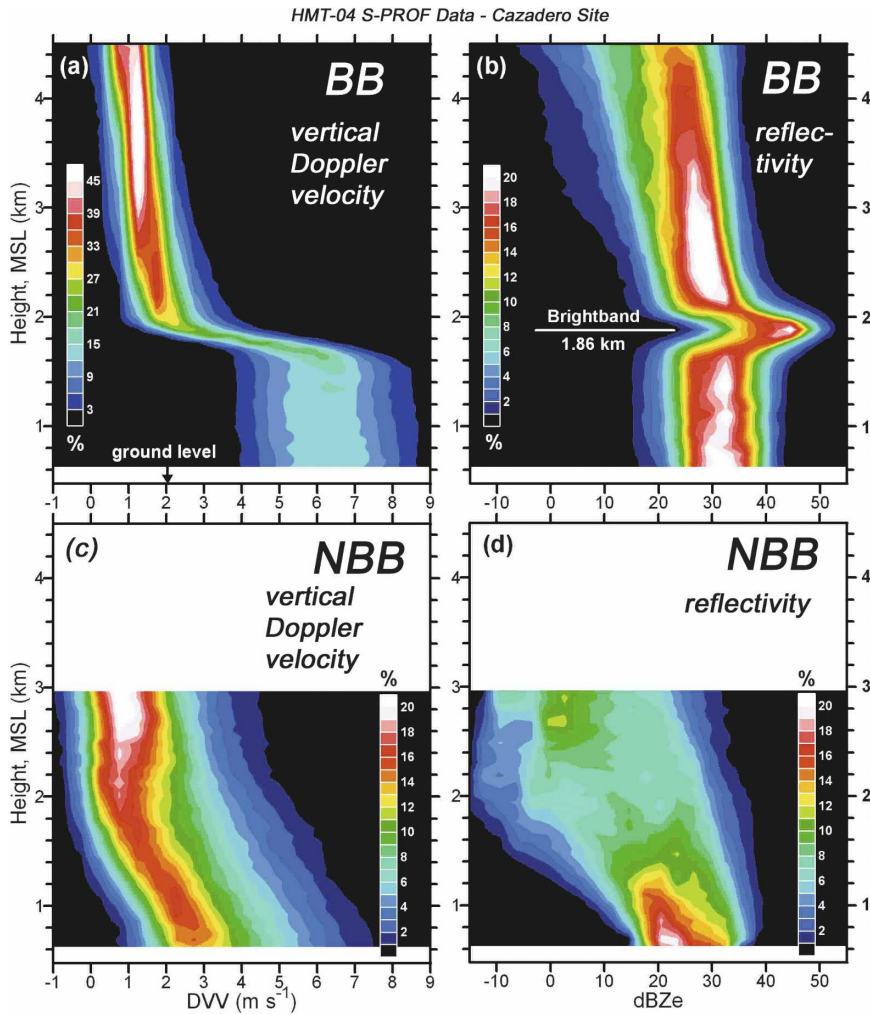


FIG. 3. Contoured frequency-by-altitude diagrams from data of the S-band profiler at Cazadero for the 2003/04 winter season. (top) Conditions during BB periods. (bottom) Corresponding conditions during NBB periods: (a) and (c) mean vertical Doppler velocity (downward positive); (b) and (d) radar reflectivity factor. The average BB height for the entire season, indicated by the white line in (b), was used to normalize the BB profile heights.

for both instruments. This resulted in adding 7 dB to the radar values. As in the earlier S-PROF studies, each BB profile was normalized by adjusting the height so that the bright band occurred at the range gate closest to the average height of the bright band for the entire season. The BB profiles are distinguished by a prominent reflectivity maximum and an abrupt increase in downward Doppler velocities beneath it. The vertical gradients of reflectivity and velocity are the key features that the algorithm of White et al. (2003) uses with the individual profiles to objectively identify BB situations and determine the brightband altitude. In contrast, the NBB profiles, which are not normalized, display a gradual increase of both parameters with decreasing height.

The JWD data for the entire winter season were sorted into BB or NBB files, according to the S-PROF classification for the half-hour segments in which they occurred. Table 1 lists the dates included in the study and the number of classified half-hour periods for each site and day. The daily rainfall accumulation associated with each rain type is also shown. The effect of orographic enhancement on precipitation can be seen by comparing daily accumulation numbers for CZD and BBY.

For the purposes of examining DSD characteristics,  $Z-R$  relations, and statistics of various rainfall parameters derived from the size spectra, the raw 1-min JWD data were integrated into 10-min samples, as in Hagen and Yuter (2003). This reduces statistical uncertainties

TABLE 1. Number of half-hour periods ( $n$ ) classified as BB and NBB, and associated rain accumulations ( $A$ ). Here, U = data unavailable on this date due to power failure at the site.

Date	BBY				CZD			
	BB	NBB	BB	NBB	BB	NBB	BB	NBB
	$n$	$n$	$A$ (mm)	$A$ (mm)	$n$	$n$	$A$ (mm)	$A$ (mm)
11 Dec 2003	0	2	0.0	0.9	U	U	U	U
12 Dec 2003	3	8	4.9	21.0	U	U	U	U
13 Dec 2003	11	2	17.4	2.9	13	23	22.2	12.4
14 Dec 2003	5	3	6.2	1.2	5	14	9.0	38.2
19 Dec 2003	U	U	U	U	7	1	11.2	0.9
20 Dec 2003	U	U	U	U	6	6	14.0	6.7
21 Dec 2003	U	U	U	U	1	4	0.6	3.8
23 Dec 2003	U	U	U	U	16	6	27.7	5.8
29 Dec 2003	12	15	14.5	19.2	10	27	43.6	72.8
30 Dec 2003	1	0	0.4	0.0	0	0	0.0	0.0
01 Jan 2004	18	3	24.1	0.8	18	7	59.7	21.4
02 Jan 2004	6	0	9.6	0.0	6	0	7.5	0.0
07 Jan 2004	4	15	3.4	10.0	5	7	6.9	3.7
08 Jan 2004	0	3	0.0	2.1	0	13	0.0	8.5
09 Jan 2004	1	6	1.1	13.0	2	6	6.9	17.2
14 Jan 2004	2	0	1.5	0.0	4	2	2.8	1.4
24 Jan 2004	2	3	2.0	1.8	2	7	2.7	9.3
27 Jan 2004	0	17	0.0	6.3	0	29	0.0	45.5
30 Jan 2004	0	2	0.0	1.1	0	3	0.0	1.3
01 Feb 2004	2	1	1.1	0.5	0	0	0.0	0.0
02 Feb 2004	7	3	14.5	2.4	13	5	34.4	9.3
03 Feb 2004	5	0	3.6	0.0	16	9	16.5	9.2
06 Feb 2004	0	0	0.0	0.0	0	2	0.0	1.8
07 Feb 2004	0	4	0.0	2.8	1	3	0.6	3.8
13 Feb 2004	2	4	2.7	3.5	3	2	4.0	1.9
14 Feb 2004	0	0	0.0	0.0	1	3	0.7	1.8
15 Feb 2004	0	0	0.0	0.0	3	0	2.1	0.0
16 Feb 2004	22	11	61.1	21.5	23	11	80.4	18.4
17 Feb 2004	6	11	11.0	7.6	13	21	36.0	42.1
18 Feb 2004	2	3	1.0	2.7	1	5	2.3	4.9
22 Feb 2004	0	0	0.0	0.0	0	1	0.0	0.2
24 Feb 2004	0	2	0.0	0.8	1	6	1.4	12.6
25 Feb 2004	10	3	23.8	3.4	17	3	63.3	4.6
26 Feb 2004	2	1	1.3	0.8	6	0	8.2	0.0
27 Feb 2004	1	0	0.6	0.0	1	0	1.3	0.0
01 Mar 2004	2	8	3.8	9.5	5	10	5.6	8.0
Totals	126	128	209.6	135.8	199	236	471.6	367.5

and biasing of  $Z-R$  relations by increasing the number of drops in each diameter bin. The instrument dead-time correction algorithm described by Sheppard and Joe (1994) and other quality controls, including requiring a minimum of 10 drops in each 1-min raw sample, were applied to the 10-min data. If individual minutes within the 10-min sample failed the 10-drop minimum requirement, those minutes were not included in DSD averaging; this occurred in less than 6% of the samples. Only periods within the half hours classified as BB or NBB were considered. Periods of very light rain or drizzle for which the data are more likely to be noisy were eliminated by requiring each half hour to have registered at least 0.5 mm of accumulation in the site's

rain gauge and each 10-min disdrometer data point to have  $R \geq 0.2 \text{ mm h}^{-1}$ .

Table 2 shows a summary of the mean values and standard deviations for several rainfall parameters derived from the DSD data for both sites. Some of the parameters are discussed briefly in this section, but all are addressed in more detail in sections 4 and 5. The entire dataset contains more than  $1.4 \times 10^7$  raindrops. The total number of 10-min data points,  $n_{10}$ , for both sites combined is 1923, representing 320.5 h of data, of which 52% were classified as NBB and 48% were BB. From the mean rain intensities,  $R$ , and  $n_{10}$ , it can be determined that NBB rain contributed 44% of the total BB + NBB rainfall accumulation at CZD and 39% at

TABLE 2. Statistics of BB and NBB rain parameters derived from the 10-min disdrometer DSD samples.

	Bodega Bay				Cazadero			
	BB		NBB		BB		NBB	
	Mean $\pm$ std dev	( $n_{10} = 354$ )	Mean $\pm$ std dev	( $n_{10} = 344$ )	Mean $\pm$ std dev	( $n_{10} = 570$ )	Mean $\pm$ std dev	( $n_{10} = 655$ )
$D_m$ (mm)	1.27 $\pm$ 0.33		0.77 $\pm$ 0.26		1.25 $\pm$ 0.35		0.73 $\pm$ 0.30	
$N_{tot}$	4186 $\pm$ 3683		7788 $\pm$ 5639		5678 $\pm$ 3422		10700 $\pm$ 5736	
Z (dBZ)	32.0 $\pm$ 5.5		25.6 $\pm$ 6.1		34.2 $\pm$ 6.1		28.0 $\pm$ 7.0	
R (mm h <sup>-1</sup> )	3.55 $\pm$ 2.77		2.37 $\pm$ 2.57		4.96 $\pm$ 4.47		3.37 $\pm$ 3.03	
log <sub>10</sub> R	0.41 $\pm$ 0.38		0.17 $\pm$ 0.43		0.52 $\pm$ 0.41		0.35 $\pm$ 0.42	
LWC (gm <sup>-3</sup> )	0.21 $\pm$ 0.16		0.22 $\pm$ 0.22		0.29 $\pm$ 0.22		0.31 $\pm$ 0.23	
$\Lambda$	3.7 $\pm$ 1.1		6.4 $\pm$ 2.1		3.7 $\pm$ 1.1		7.0 $\pm$ 2.8	
$N_0$ (m <sup>-3</sup> mm <sup>-1</sup> )	2.7 $\pm$ 8.3 ( $\times 10^4$ )		1.7 $\pm$ 2.4 ( $\times 10^5$ )		2.0 $\pm$ 3.8 ( $\times 10^4$ )		4.4 $\pm$ 7.2 ( $\times 10^5$ )	
log <sub>10</sub> ( $N_0$ )	3.90 $\pm$ 0.55		4.80 $\pm$ 0.69		4.02 $\pm$ 0.46		5.09 $\pm$ 0.77	
$N_0^*$ (m <sup>-3</sup> mm <sup>-1</sup> )	1.9 $\pm$ 5.8 ( $\times 10^4$ )		1.0 $\pm$ 1.4 ( $\times 10^5$ )		1.8 $\pm$ 3.2 ( $\times 10^4$ )		2.5 $\pm$ 3.9 ( $\times 10^5$ )	
log <sub>10</sub> ( $N_0^*$ )	3.75 $\pm$ 0.56		4.61 $\pm$ 0.67		3.92 $\pm$ 0.49		4.93 $\pm$ 0.72	
Student <i>T</i>								
<i>p</i> -01 significant?								
Student <i>T</i>								
<i>p</i> -01 significant?								

BBY. When the CV periods (not shown) are included, NBB rain contributed 40% of the winter season's rainfall at CZD and 32% at BBY. These percentages are within the ranges found by Neiman et al. (2005) in four other winters and four locations, including BBY and CZD. Thus, the dataset examined here was not exceptional in this respect.

As shown in Table 2, mean rainfall intensities,  $R$ , derived from the disdrometer data for BB periods exceeded those for NBB by a factor of 1.47 at CZD and 1.50 at BBY. Approximately the same ratios are found using the coarser-resolution rain gauge data. Thus, rainfall during BB periods was, on average, approximately 50% more intense than during NBB periods. The BB/NBB ratio of mean rain intensities at CZD agrees fairly well with the 1.37 ratio found by Neiman et al. (2005) for the same site in four earlier winters. Mean-volume drop diameters (or mass-weighted mean diameter),  $D_m$ , shown in Table 2, were approximately a factor of 1.7 smaller and the mean total number of drops,  $N_{tot}$ , was almost a factor of 1.9 larger for NBB compared to BB periods at both locations. Thus, nonbrightband periods had more drops, but considerably smaller ones, than brightband periods. This confirms one of the primary inferences made by White et al. (2003) from S-PROF data and without direct measurements of drop sizes.

#### 4. Comparison of DSDs

DSDs from the individual 10-min samples were averaged for the entire winter season to derive mean size spectra for both types of rain. Although individual 10-min DSDs varied widely and were often not exponential in shape, the season-average DSDs are approximately exponential. Application of the instrument's dead-time corrections increased the concentrations [ $N(\text{m}^{-3} \text{mm}^{-1})$ ] of very small drops compared to the raw spectra, but generally had little effect on the concentrations of drops with diameters ( $D$ ) exceeding about 0.5 mm. Changes caused by application of the dead-time correction to rainfall parameters derived from the DSDs were far smaller than differences between these parameters for BB and NBB periods. The resulting season-average drop size spectra are shown in Figs. 4 and 5.

Figure 4 shows the mean size spectra in their basic, unnormalized form for the entire winter for both rain types at both sites. At both locations the NBB spectra contained larger concentrations of small drops ( $D < 1$  mm) and much smaller concentrations of large drops ( $D > 2$  mm) than the BB rainfall. Drop concentrations in the two types of rain were equal at approximately  $D = 1$  mm, but the slope of the spectra was considerably greater for NBB periods. The NBB concentrations

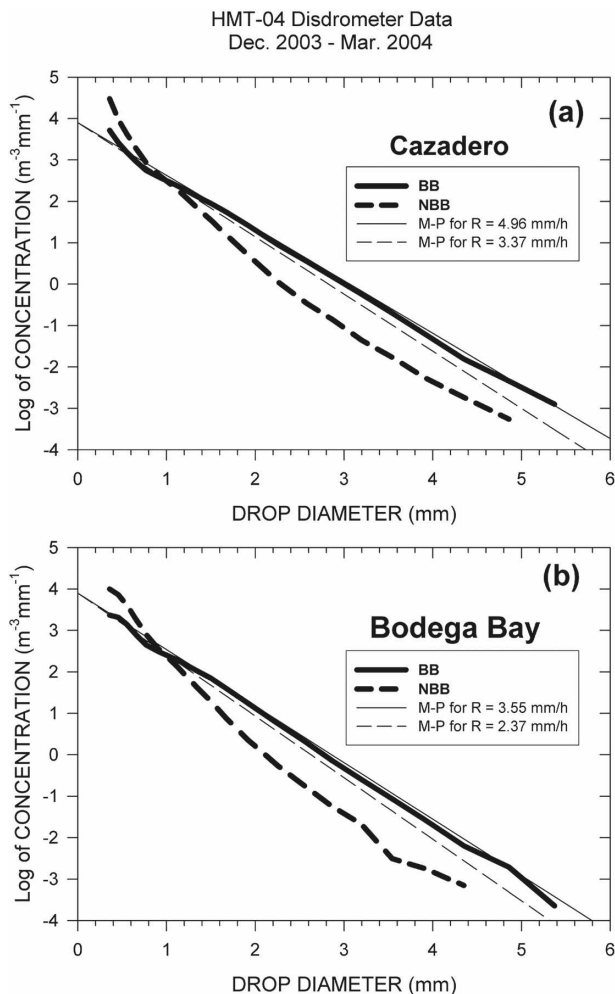


FIG. 4. Mean drop size distributions at (a) Cazadero and (b) Bodega Bay derived from the 10-min disdrometer samples for the HMT-04 winter season. Heavy lines are the measurements for BB (solid) and NBB (dashed) periods. Thin straight lines are the exponential M-P spectra for the same average rainfall intensities as the HMT-04 observations, where the thin solid lines correspond to the BB rain rates at each site and the thin dashed lines correspond to the NBB rain rates.

exceeded those of BB by a factor of 3 or more for  $D < 0.6$  mm. NBB concentrations were almost a factor of 10 lower than those of BB rain for  $D > 2$  mm. Three decades earlier, Waldvogel (1974) reported similar large-drop–small-drop DSD differences in the presence/absence of a bright band for one day of orographic rain in Switzerland.

Comparisons with the well-known drop size distributions of Marshall and Palmer (1948) are also shown in Fig. 4. Marshall and Palmer (M-P) sampled primarily stratiform rainfall in southeastern Canada. They used an exponential Eq. (1) to describe how drop concentrations varied with drop size in their data:

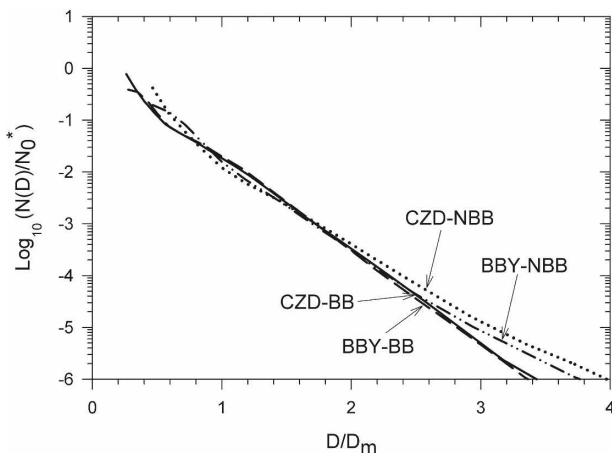


FIG. 5. Normalized drop size distributions from the disdrometer measurements during BB and NBB periods at Cazadero and Bodega Bay. The normalizations use the method of Testud et al. (2001).

$$N = N_0 e^{-\Lambda D}, \tag{1}$$

where the y axis intercept is a constant ( $N_0 = 8 \times 10^3$ ), and the slope is a function of rain rate ( $\Lambda = 4.1R^{-0.21}$ ). Units are  $m^{-3} mm^{-1}$  for  $N$  and  $N_0$ ,  $mm h^{-1}$  for  $R$ ,  $mm$  for  $D$ , and  $mm^{-1}$  for  $\Lambda$ . The M-P curves shown in Fig. 4 were computed from Eq. (1) using the HMT-04 whole-season mean  $R$  values from the JWD data at CZD and BBY for the BB and NBB conditions, as shown in Table 2 and in the figure. The BB data match the M-P spectra very closely. In contrast, the NBB data contain greater concentrations of small drops and much smaller concentrations of large drops than the corresponding M-P spectra for the same rain intensity. Thus, the M-P equation closely approximates the observed BB rainfall, but poorly represents the NBB observations.

It should be noted, however, that it is difficult to make reliable interpretations of differences among unnormalized spectra, such as those in Fig. 4, because drop concentrations are generally a function of rain intensity, and the season-average  $R$  values for the HMT-04 BB/NBB spectra differ by as much as 50% (Table 2). Therefore, normalizations of the HMT-04 DSD data are presented in Fig. 5, using the procedures of Testud et al. (2001). Their method, which is independent of assumptions about the shape of observed drop spectra, is helpful for comparing DSDs from different rain types or different studies and for examining them for indications of differences in the physical processes that produced the rain. Additionally, this normalization removes the dependence of concentration on  $R$  at a particular diameter. The diameter ( $x$  axis) data in these

plots are normalized by  $D_m$ , and the concentration data ( $y$  axis) are normalized by the parameter  $N_0^*$ , which is proportional to the spectra's liquid water content (LWC) and inversely proportional to  $D_m^4$ .

Figure 5 shows almost no difference in the normalized BB spectra at the BBY and CZD sites, suggesting that the BB rain production process is essentially the same at the shoreline and in the coastal mountains. The BB data are also in close agreement with the mean normalized spectra presented by Testud et al. (2001) for stratiform rainfall over the western Pacific Ocean. The NBB curves in Fig. 5, however, depart noticeably from the BB data for  $D/D_m > 2$ , with the NBB curve for CZD showing the greatest departure. This suggests physical differences in the character of NBB rain periods, which are responsible for producing smaller  $D_m$  and much larger  $N_0^*$  values, yet similar LWC values (Table 2) compared to its BB counterpart. The greater departure for the CZD site suggests that localized orographic processes may be important in the production of rainfall during NBB periods, as was found by Neiman et al. (2005) for northern California. Levin et al. (1991) also noted orographic effects in drop spectra from mountainside measurements in Switzerland. The NBB values of  $N_0^*$  are also considerably larger than those observed by Testud et al. (2001) for either stratiform or convective rain types in the western Pacific.

## 5. Frequency distributions of rainfall and echo-top parameters

### a. Rain parameters

The different DSDs for BB and NBB periods produce contrasts in rain parameters derived from the DSDs, as shown in Table 2. These differences are further revealed in the frequency distributions of Fig. 6, which are based on the hundreds of individual 10-min samples from the disdrometers, with the data combined from both sites. Distributions of  $Z$ ,  $R$ ,  $D_m$ , total number of drops ( $N_{\text{tot}}$ ), slope of the drop spectra ( $\Lambda$ ), and LWC are shown for both rain types. Compared with the BB distributions, the NBB distributions are shifted toward considerably lower reflectivities, lower rain intensities, much smaller mean-volume diameters, greater total numbers of drops, and larger (steeper) DSD slopes (Figs. 6a–e). Although these distributions overlap, the two-tailed Student's  $t$  test shows the difference of the BB and NBB means are statistically significant at the  $p = 0.01$  level of significance (99% confidence level). Table 2 shows the statistics (for each site separately), where it can be seen that, compared to BB periods, the NBB periods have mean values that are roughly 6 dB

lower for  $Z$ , 32% lower for  $R$ , 40% smaller for  $D_m$ , 87% greater for  $N_{\text{tot}}$ , and 81% larger for  $\Lambda$ .

The differences for LWC (Fig. 6f), however, are small (means differ by  $\sim 6\%$ ), and not statistically significant. Thus, DSDs differ between BB and NBB periods in such a way that their mean values of  $D_m$ ,  $N_{\text{tot}}$ ,  $Z$  (proportional to  $D^6$ ), and  $R$  (proportional to  $\sim D^{3.7}$ ) are significantly different, but their LWC values (proportional to  $D^3$ ) are essentially the same. This may occur if the DSDs are similar across the middle range of drop sizes, but are quite different at smaller and larger drop sizes. The statistical tests bolster conclusions from the earlier PACJET/CALJET studies that different physical processes are involved in the development of NBB and BB rainfall.

In analyses (not shown) of HMT-04 DSD variability, similar to those of Steiner et al. (2004), the NBB variability was found to be more strongly controlled by changes in the total number of drops than was true for BB periods, where changes in drop sizes are more influential. It was also found that, unlike BB periods, increases of LWC within the NBB dataset were uncorrelated with  $D_m$ . Thus, in NBB situations, increases of LWC were primarily the result of greater drop concentrations rather than increased drop sizes.

### b. Echo-top conditions

The radar bright band, exhibited by all BB cases, is definitive evidence of the presence of ice crystals and melting aloft. Echo tops of all BB cases extend above the  $0^\circ\text{C}$  level. Although the NBB cases do not exhibit a melting-layer bright band, their echoes usually also extend above the melting layer. Those NBB clouds almost certainly do not contain large ice crystals. They are either composed entirely of water droplets (supercooled above the  $0^\circ\text{C}$  altitude), or they may also contain ice crystals that are too small to produce the large increase of fall speed upon melting that is required to meet the objective BB profile criteria of White et al. (2003).

The S-PROF echo-top data were analyzed to further quantify BB/NBB differences. Statistics on the extent of the echo-top heights above the  $0^\circ\text{C}$  level contain information about whether the presence of ice in NBB cases is plausible, because ice nucleation becomes more effective as clouds extend to higher, colder altitudes. Information about how echo-top heights were related to the height of the  $0^\circ\text{C}$  level was derived by combining S-PROF and radiosonde data. Temperature-aloft data were obtained from serial radiosondes launched by HMT from the nearby FRS site (see Fig. 1) within 6 h of the S-PROF and disdrometer data. This was possible for 50% of the half hours classified as BB or NBB. Only

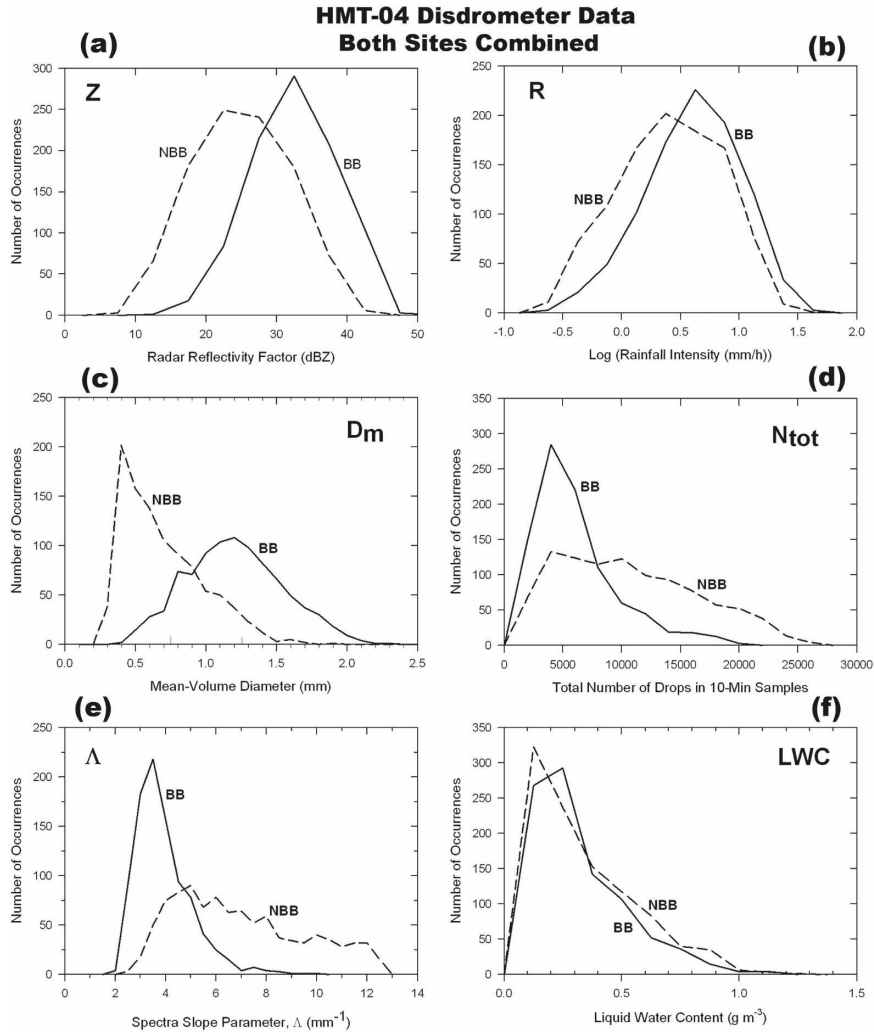


FIG. 6. Frequency distributions of various parameters computed from the DSDs measured by the disdrometers. Each unit on the y axis represents one 10-min sample. Parameters are (a) reflectivity, (b) rainfall intensity, (c) mean-volume diameter, (d) total number of drops, (e) slope of the drop size spectrum, and (f) liquid water content.

S-PROF and sonde data from that half of the full dataset were used in the echo-top analyses. Based on experienced data inspection, the S-PROF echo-top height was specified as the height at which the instrument’s signal-to-noise ratio fell below  $-14$  dB (approximately  $-1$  dBZ at 8 km AGL). These echo-top data underestimate cloud-top heights to an unknown degree because the instrument’s sensitivity, although impressive, is limited, and the recorded data were truncated at 8 km AGL.

Figure 7a shows histograms of echo-top temperature, using combined datasets from CZD and BBY. There is a wide separation in the peaks of the two distributions ( $-32.5^{\circ}\text{C}$  for BB and  $-2.5^{\circ}\text{C}$  for NBB). Figure 7b presents distributions of the height of the echo tops above

the  $0^{\circ}\text{C}$  level, or the thickness of the subfreezing echo layer. It shows that, although most NBB and all BB periods had echo tops that extended upward into subfreezing altitudes, the NBB cases usually did not extend nearly as far into those cold altitudes. Approximately 15% of the NBB periods had echo tops below the  $0^{\circ}\text{C}$  isotherm, and thus, definitely contained no ice crystals. For the remaining 85%, however, the clouds extended into freezing altitudes, even though no bright band was detected. Of course, none of the BB cases had tops warmer than  $0^{\circ}\text{C}$ , and all contained ice.

The mean echo-top height was 6.8 km (corresponding to  $-26.3^{\circ}\text{C}$ ) for BB periods but only 3.6 km ( $-5.6^{\circ}\text{C}$ ) for NBB; the difference is statistically significant at the  $p = 0.01$  level. Only 22% of the NBB cases

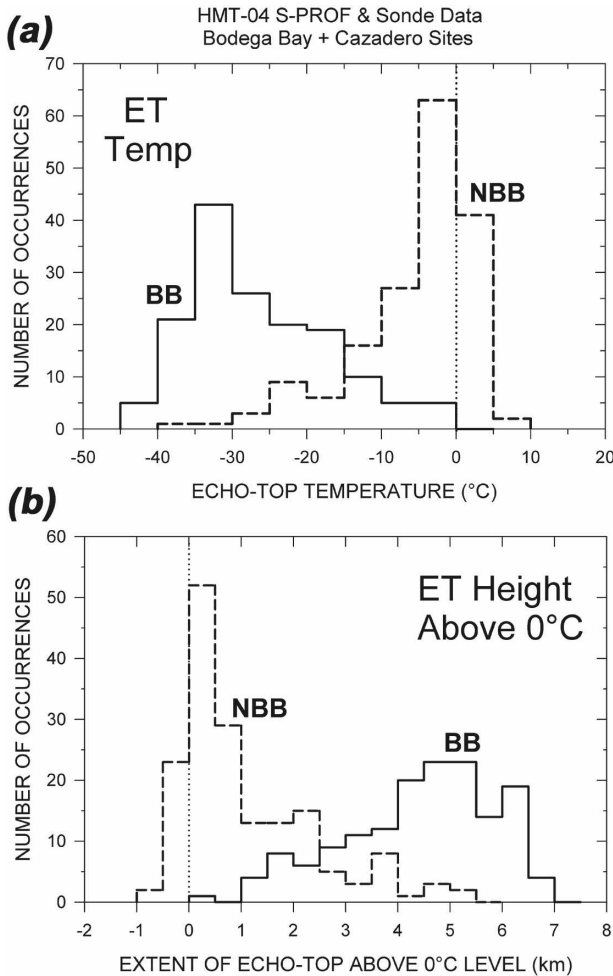


FIG. 7. Histograms of (a) echo-top temperature and (b) echo-top height above the 0°C altitude. Echo-top data are from S-PROF measurements at CZD and BBY, and temperature data are from nearby radiosonde data at FRS.

had echo tops located more than 2 km above the 0°C level, compared to 92% for BB cases. The mean height of the NBB echo tops above the 0°C isotherm was only 1.1 km, compared with approximately 4.4 km for BB. The mean echo-top temperature NBB–BB difference of approximately 21°C agrees well with the 20-K difference in cloud-top infrared temperatures found by Neiman et al. (2005) at CZD during four other winters, although their cloud-top temperatures were colder than the echo-top temperatures of this study.

In Fig. 8 disdrometer, S-PROF, and sounding data are combined to illustrate the relation between echo-top height and drop size. In both BB and NBB periods,  $D_m$  increases as the height of the echo top above the 0°C level increases. During BB periods, thicker cloud layers above the 0°C level allow more time for falling ice crystals to grow by vapor deposition, and more op-

portunities for riming and aggregational growth. These ice particles become large raindrops upon melting. During NBB periods, thicker cloud layers allow for enhanced growth of supercooled raindrops by condensation and coalescence. The separation of BB and NBB points is clearest in the upper-right and lower-left shaded portions of the diagram. For points with  $D_m > 1.5$  mm, 91% had echo tops that extended more than 3 km above the 0°C level, and of those, 98% were BB situations. For points with  $D_m < 1.0$  mm, 68% had echo tops that extended less than 2 km above the 0°C level, and of those, 93% were NBB situations. Thus, high, cold echo-top clouds almost always produced larger hydrometeors and a bright band, but, low, warm echo-top clouds almost always failed to generate large drops and a bright band. In intermediate regions of the diagram there is more overlap of points and the BB/NBB separation is less clear. But the general trend is still apparent: higher echo tops are usually associated with larger drops and the presence of a bright band.

The difference in echo-top heights implies that ice processes are much more likely to be a controlling microphysical factor in the production of BB precipitation production, and they may often be entirely absent in NBB precipitation cases. The shallowness of NBB periods poses additional challenges for monitoring these conditions over Sonoma County with the operational NEXRAD radars, which are too far away for their lowest scans to detect much of any storm's low-altitude (<3 km MSL) echo (White et al. 2003).

## 6. Comparison of $Z$ – $R$ relations

The 10-min-sample DSD datasets from the HMT-04 disdrometer measurements were used to compute  $Z$  ( $\text{mm}^6 \text{m}^{-3}$ ) and  $R$  ( $\text{mm h}^{-1}$ ) for BB and NBB periods, assuming Rayleigh conditions for the computation of  $Z$ . Regressions of the scatter of  $(Z, R)$  points were computed for both sites in the traditional form,  $Z = aR^b$ . However, recent studies by Ciach and Krawjowski (1999), Campos and Zawadzki (2000), Steiner and Smith (2000), and Tokay et al. (2001) caution that  $Z$ – $R$  equations are method-dependent and can be quite sensitive to details of the regression technique. This makes it difficult to assess physical process differences when comparing  $Z$ – $R$  relations from different studies, because many earlier articles have not documented the methods they used. In the present work,  $R$  was treated as the dependent variable, and the regression was computed as the least squares fit to the  $\log R$  versus  $10 \log Z$  ( $= \text{dBZ}$ ) data. A lower cutoff threshold of  $R > 0.2 \text{ mm h}^{-1}$  was employed to eliminate points of very light, and possibly noise-contaminated, rain. Exactly the same method was applied to the BB and NBB cases.

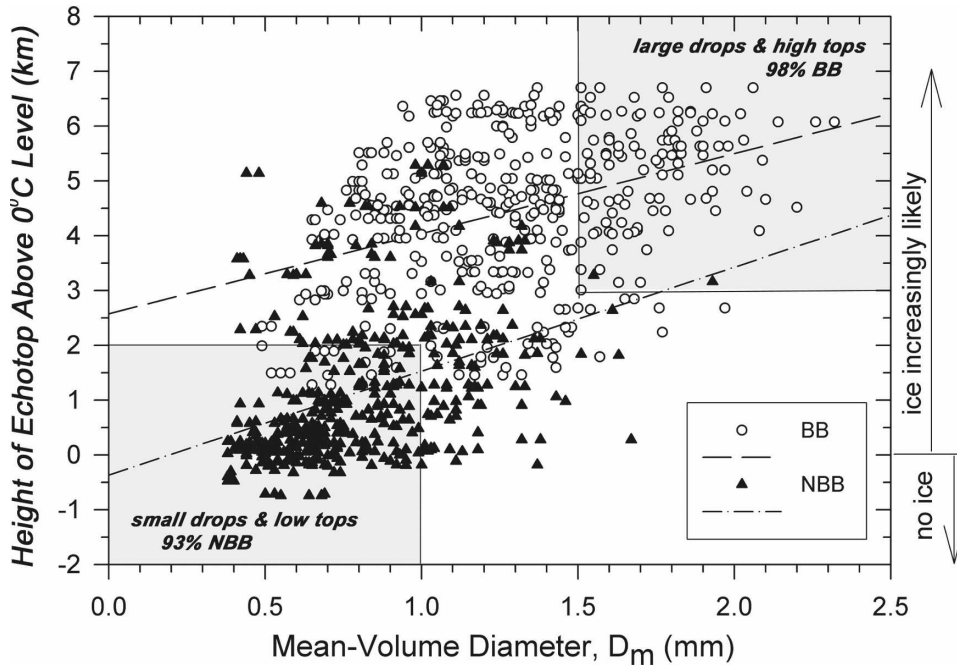


FIG. 8. Mean-volume drop diameter measured by the disdrometers as a function of height of the S-PROF echo top above the 0°C level. Data from Cazadero and Bodega Bay for BB (open circles) and NBB (triangles) periods are included. Each point represents one 10-min disdrometer sample. Dashed lines are least squares best fits to the data.

Figure 9 shows the JWD scatterplots and regressions for the two disdrometer locations, with the resulting regression equations shown in the figure and in Table 3. The correlation coefficient for the regression data exceeds 0.86 for both locations and both rainfall types. Although there is a large amount of overlap, it is clear that the NBB points occurred with generally lower reflectivity than their BB counterparts for similar rain intensities. At both locations the coefficient,  $a$ , of the regression equation is considerably smaller for NBB rainfall. This agrees with the earlier findings of White et al. (2003) and Kingsmill et al. (2006), based on radar profiler and rain gauge data. The regressions for BB rainfall are very similar at CZD and BBY.

Some researchers, including Hagen and Yuter (2003), Doelling et al. (1998), and Steiner and Smith (2000) favor a simplification in deriving  $Z-R$  relations, which constrains the exponent to a reasonably representative constant value, such as  $b = 1.5$ . Smith and Joss (1997) argue that this approach yields good results for applications involving radar estimations of rainfall accumulations, even if the estimations of instantaneous rain rates are not impressive. This constrained-exponent method also has the advantage of allowing simple statistical significance tests on the resulting frequency distributions of the coefficient,  $a$ . For the HMT-04 disdrometer dataset, this method was applied using

$b = 1.6$ , which closely matches the values shown in Fig. 9 for the BB rainfall. The coefficients were computed from the DSD datasets as  $a = ZR^{-1.6}$ . The resulting exponent-constrained  $Z-R$  relations are shown in Table 3 for both sites, and histograms of the coefficient are shown for the CZD site in Fig. 10. It again can be seen that the coefficient is considerably smaller during NBB periods; the mean BB-NBB coefficient difference is statistically significant at the  $p = 0.01$  level. At CZD, where orographic forcing is stronger, the constrained relation is  $Z = 166 R^{1.6}$  for BB periods, compared to  $Z = 56 R^{1.6}$  for NBB periods, with standard deviations of  $\pm 2$  for the coefficients.

The  $Z-R$  relations were also derived from the data of S-PROF (for  $Z$ ) and rain gauge (for  $R$ ) during HMT-04. The processing was essentially the same as that used by White et al. (2003), although they used  $Z$  instead of  $R$  as the dependent variable in their regressions. The BB and NBB time periods are the same as those used with the disdrometer data, but fewer points are available because the radar (and disdrometer) averaging interval is 30 min, instead of 10. The reflectivity data were obtained at 210 m AGL, which was considered to be the lowest useable range gate for these datasets. A lower cutoff threshold of  $R > 1 \text{ mm h}^{-1}$  was used to eliminate noisy radar and gauge points. The resulting S-PROF/gauge-based  $Z-R$  equations are shown in

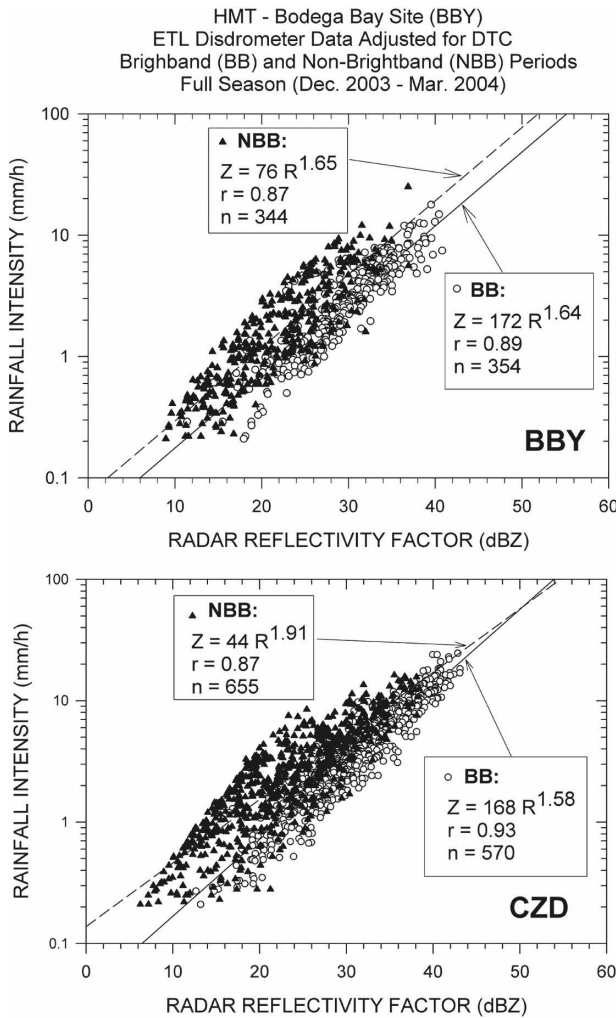


FIG. 9. Scattergrams of  $Z$ - $R$  and best-fit regressions for the disdrometer data from (top) Bodega Bay and (bottom) Cazadero. BB periods are shown by open circles and NBB periods by triangles. Each point represents one 10-min integration of disdrometer data.

TABLE 3. HMT-04  $Z$ - $R$  relations ( $Z = aR^b$ ) derived from disdrometer data and from S-band profiler and rain gauge data for BB and NBB periods at Cazadero and Bodega Bay.

	BB		NBB					
	CZD		BBY		CZD		BBY	
	$a$	$b$	$a$	$b$	$a$	$b$	$a$	$b$
Disdrometer	168	1.58	172	1.64	44	1.91	76	1.65
Disdrometer (constrained exponent)	166	1.60	182	1.60	56	1.60	77	1.60
S-PROF*/gauge	210	1.46	175	1.94	35	1.77	50	1.98

\* The S-PROF reflectivity data include a calibration adjustment of +7dB, based on the concurrent disdrometer data.

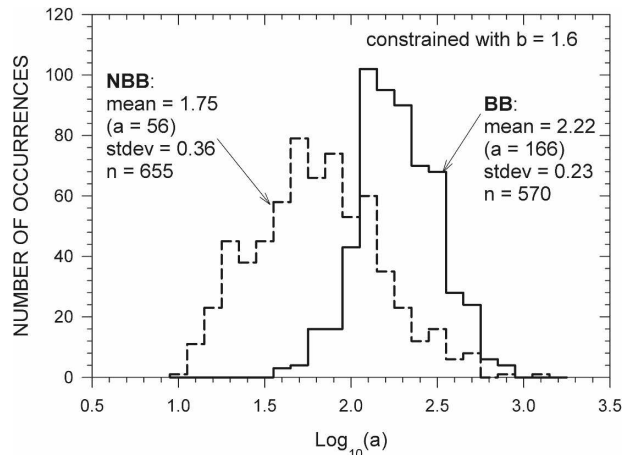


FIG. 10. Histograms of the coefficient for coefficient of  $Z = aR^b$  relations computed from the disdrometer measurements at CZD, using a constrained value of  $b = 1.6$ .

Table 3 along with those derived from the disdrometer data. Although the exponents vary in the table, a consistent feature at both sites and from all three methods is that the coefficient is considerably smaller for NBB rainfall compared to BB rain. This feature agrees with the results of the earlier CALJET and PACJET investigations.

NWS personnel have the ability to select among various  $Z$ - $R$  relations for the NEXRAD radars, to suit local and seasonal weather situations. Radar-based rainfall accumulations are then routinely estimated by application of these equations. Three relations prominently recommended in NWS training courses are tested here using the HMT-04 disdrometer observations. These include relations recommended for nontropical convective precipitation ( $Z = 300R^{1.4}$ , sometimes referred to as the “standard” NEXRAD relation), stratiform and orographic precipitation ( $Z = 200R^{1.6}$ ; from Marshall and Palmer 1948), and for western United States cool-season precipitation ( $Z = 75R^{2.0}$ ). The first two relations are heavily used throughout the NEXRAD network. The M-P relation was used for the entire HMT-04 winter by the Santa Clara County NEXRAD (KMUX) near San Francisco (D. Reynolds 2005, personal communication).

An assessment of the degree to which the NEXRAD relations match the observed rainfall is presented in Table 4, in terms of total-season accumulations for the two rain types. The  $Z$  values from the disdrometers’ 10-min samples were used in the three NEXRAD equations to estimate  $R$ , which was then converted to accumulation by time integration. The table shows that at both BBY and CZD the nontropical convective “standard” relation and the M-P relation recommended for

TABLE 4. Rainfall accumulations observed by the disdrometers and retrieved from  $Z$ - $R$  relations commonly used by NEXRAD operational radars. The disdrometer-observed population of  $Z$  values was used as input to the NEXRAD  $Z$ - $R$  equations. Data include the full winter season (December 2003–March 2004), using the 10-min disdrometer samples, excluding points with  $R < 0.2 \text{ mm h}^{-1}$ . Percentages of the disdrometer-observed accumulation are shown in parentheses.

Accumulations observed by disdrometer	Accumulations from $Z$ - $R$ relations commonly used with NEXRAD		
	Nontropical convection ( $Z = 300R^{1.4}$ )	Stratiform and orographic (M–P) ( $Z = 200R^{1.6}$ )	Western U.S. cool season ( $Z = 75R^{2.0}$ )
BB, Bodega Bay: 209.6 mm (100%)	173.3 mm (83%)	188.4 mm (90%)	234.1 mm (112%)
BB, Cazadero: 471.6 mm (100%)	386.8 mm (82%)	399.8 mm (85%)	464.6 mm (99%)
NBB, Bodega Bay: 135.8 mm (100%)	55.6 mm (41%)	68.4 mm (50%)	101.8 mm (75%)
NBB, Cazadero: 367.5 mm (100%)	152.8 mm (42%)	177.7 mm (48%)	245.2 mm (67%)

stratiform and orographic precipitation underestimated the actual full-season BB rain accumulations by a modest 10%–18%. The western U.S. cool-season relation underestimated BB accumulations by only 1% at CZD and overestimated them by 12% at BBY. In general, these are probably not serious differences from the observed BB rain data.

Comparisons with the NBB observations were much poorer, however. Table 4 shows that the NEXRAD nontropical convective and stratiform/orographic  $Z$ - $R$  relations underestimated actual season-total NBB rainfall accumulations by a factor of 2 or more. The western U.S. cool-season relation was somewhat better, but still underestimated NBB accumulations by 25% at BBY and by 33% at CZD. Thus, although these NEXRAD relations may be appropriate for the BB rainfall periods, their use results in very sizable underestimates of rainfall during NBB situations. Of course, these results are based on the observed DSD data with  $Z$  and  $R$  derived from the same instrument, and it should be noted that additional sources of error may arise when comparing actual radar measurements of  $Z$  and rain gauge measurements of  $R$ .

The NBB  $Z$ - $R$  relations from HMT-04 resemble those of Blanchard (1953) for orographic rain in Hawaii, and support other studies, such as Amitai (2000) in Australia, where unusually large rain rates for a given  $Z$  were found for stratiform rain without a bright band. Based on these findings, the operational hydrometeorologist should be aware that conventional radar methods may seriously underestimate nonconvective rain accumulations when a bright band is not present. Armed with this knowledge, the challenge is then to identify NBB conditions and to apply more appropriate  $Z$ - $R$  equations, such as those derived from the HMT-04 disdrometer data.

## 7. Polarimetric radar applications

As has been demonstrated, the S-PROF instrument provides useful information about precipitation conditions aloft at their point locations. Unlike scanning radars, however, they provide no area coverage. On the other hand, although it is fairly easy to identify melting-layer bright bands using the reflectivity and Doppler data of the vertically pointing profiling radars (White et al. 2002), it is often difficult to determine whether a bright band is present using reflectivity or Doppler data from the low-elevation sweeps of scanning radars. Brandes and Ikeda (2004) and Matrosov et al. (2007) offer more robust methods for delineating the location of bright bands using data from polarimetric scanning radars. The current network of NEXRAD radars does not yet have dual-polarization capability, but it is scheduled to be added in the next few years. Therefore, it is useful to briefly explore whether measurements available from polarimetric scanning radars may also offer promise for identifying and distinguishing between BB and NBB rain types. In this way, it may be possible to extend the point-specific information of S-PROF to much larger regions.

Polarimetric radars are sensitive to drop shapes or hydrometeor axial ratio. The greater abundance of small drops in NBB rain implies that its drop shapes are more nearly spherical than for BB rainfall. Thus, polarimetric radar may be able to detect useful distinctions in the two rainfall types. Polarimetric radar methods are also capable of providing more accurate estimates of rainfall intensity and accumulation than is generally possible with  $Z$ - $R$  methods, which suffer from many weaknesses (Zrnić and Ryzhkov 1996).

The polarimetric parameters, specific differential propagation phase shift,  $K_{DP}$  ( $^{\circ} \text{ km}^{-1}$ ), and differential

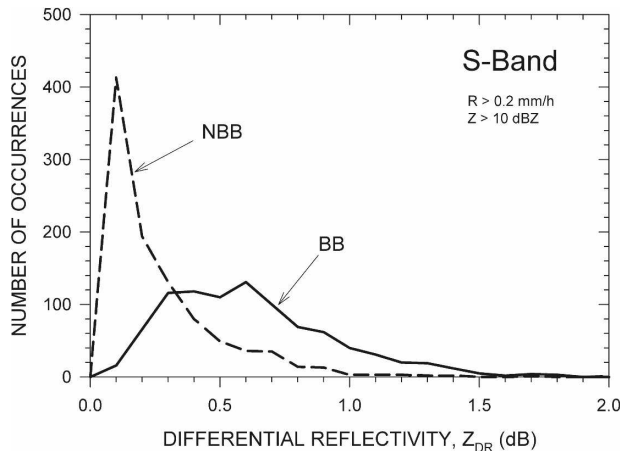


FIG. 11. Combined-site frequency distributions of differential reflectivity computed from the 10-min disdrometer measurements at Cazadero and Bodega Bay. The  $Z_{DR}$  data are for S-band radar wavelengths.

reflectivity,  $Z_{DR}$  (dB), were computed from the 10-min DSDs measured by the HMT-04 disdrometers, following the method described in Matrosov et al. (2005) and using the relation of Brandes et al. (2004) between drop diameter and axial ratio. In addition to the S-band ( $\lambda \sim 11$  cm) wavelength used by NEXRAD, these computations were also made for X-band radar wavelengths ( $\lambda \sim 3$  cm).

#### a. Classification of BB and NBB rainfall using $Z_{DR}$

Although  $Z_{DR}$  is used by some radar meteorologists in algorithms for estimating  $R$ , it is probably more commonly employed to classify hydrometeor types, such as for distinguishing regions of snowflakes, hail, and raindrops from each other (Bringi and Chandrasekar 2001). In this study, the even more challenging task of using  $Z_{DR}$  to distinguish between two types of rainfall is examined. The variable  $Z_{DR}$  is zero for small, spherical drops, such as those that dominate NBB size distributions, and becomes progressively larger for the more oblate shapes corresponding to large drop diameters, which are much more common in BB rainfall.

Frequency distributions of  $Z_{DR}$  computed from the HMT-04 DSD data indicate that this polarimetric parameter may have some limited usefulness for identifying and distinguishing the two types of rain. In Fig. 11, for instance, the NBB distribution is shifted, as expected, toward lower  $Z_{DR}$  values compared to the BB distribution. Only 9% of the BB cases had  $Z_{DR} \leq 0.2$  dB, and only 11% of the NBB cases had  $Z_{DR} \geq 0.6$  dB. Therefore, in spite of the overlap of the distributions shown in the figure, it is clear that if a perfectly precise polarimetric radar monitoring coastal northern Califor-

nia rain measures  $Z_{DR} \geq 0.6$  dB, it is very probably observing a BB case, and if it measures  $Z_{DR} \leq 0.2$  dB it is probably observing NBB rainfall. At intermediate values, either rain type might well be present. In practice, however, these distinctions will be blurred by the uncertainty (approximately  $\pm 0.2$  dB) in real radar measurements of  $Z_{DR}$ , and the usefulness of these classification thresholds will be reduced.

#### b. Estimating rainfall intensities with $K_{DP}$

Although researchers have developed algorithms to estimate  $R$  as a function of  $Z$ ,  $K_{DP}$ , and  $Z_{DR}$ , separately and in combinations of these parameters, we limit our attention to  $R = f(Z)$  (in section 6) and  $R = f(K_{DP})$ , which are probably the ones most commonly used. Regression equations were computed to derive  $K_{DP}$ - $R$  power-law relations in a manner analogous to the  $Z$ - $R$  equations. For a given DSD, the magnitude of the  $K_{DP}$  parameter scales approximately inversely with radar wavelength. Therefore, shorter wavelength radars, such as X-band systems, are capable of detecting smaller differential phase shifts than longer wavelength systems, such as S band (Matrosov et al. 2005). Unfortunately, in NBB rainfall, the vast majority of the  $K_{DP}$  values computed from the observed DSDs are so small that they would be very difficult to detect with almost any polarimetric radar. Typically,  $K_{DP}$  values less than about  $0.1^\circ \text{ km}^{-1}$  are so small that they are within the measurement noise of polarimetric radars, and are therefore not reliable for estimating rainfall rates (Matrosov et al. 2006). However, only 1% of the NBB cases from HMT-04 had  $K_{DP} \geq 0.1^\circ \text{ km}^{-1}$  for S band, and the number is not much better (12%) for X-band frequencies (see Fig. 12b). Thus, in practice,  $K_{DP}$  will not generally be useful for estimating  $R$  in NBB cases, even with the more sensitive X-band radars. The more traditional reflectivity-based  $Z$ - $R$  estimates, in spite of their shortcomings, must still be employed for NBB rain.

The situation is somewhat more promising for BB rainfall (Fig. 12a) because of the presence of greater numbers of larger, more flattened drops. However, even in the BB cases, most of the HMT-04 DSD data points were for light rain rates, in which the concentrations of large drops are not particularly high. Consequently, only 12% of the BB data points had  $K_{DP} \geq 0.1^\circ \text{ km}^{-1}$  for S-band frequencies. Thus,  $K_{DP}$ - $R$  methods are unlikely to be useful for S-band polarimetric radar in either BB or NBB rain in northern California. For the more sensitive X-band frequencies, 44% of the DSD points in BB rain exceeded the  $K_{DP} = 0.1^\circ \text{ km}^{-1}$  detection threshold. This was a large enough number to obtain meaningful regressions with high correlations.

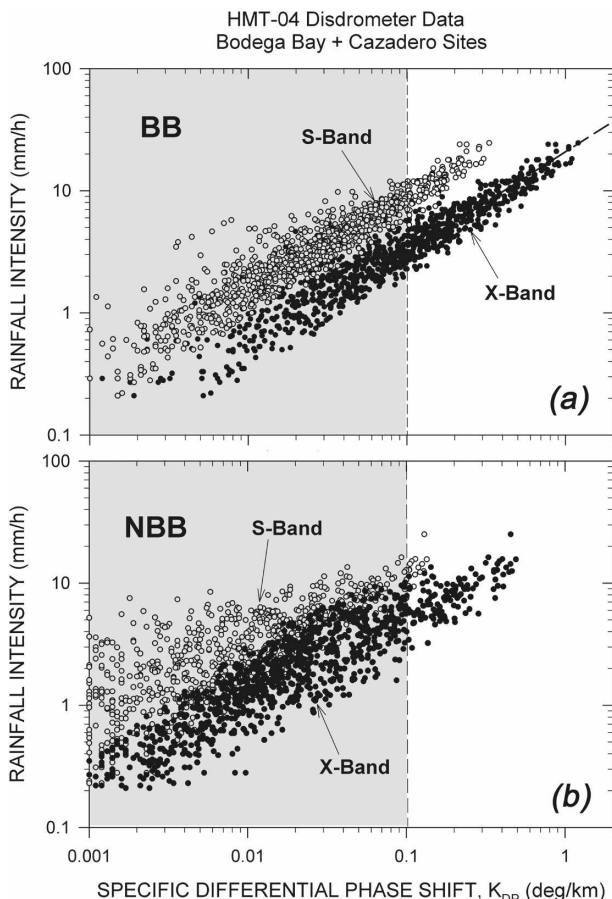


FIG. 12. Rainfall intensity as a function of specific differential phase shift,  $K_{DP}$ , for (a) BB and (b) NBB periods. Each point represents one 10-min disdrometer sample. Black dots are for X-band radar wavelengths; open circles are for S band. Polarimetric radar measurements for approximately  $K_{DP} < 0.1^\circ \text{ km}^{-1}$  (shaded region) are expected to be too noisy for practical use.

The regressions were nearly identical for CZD and BBY, and X-band power-law relation is  $R = 18 K_{DP}^{0.71}$  when the data from both sites are combined. This equation is similar to the one derived by Matrosov et al. (2005) for five individual HMT-04 days that were predominantly BB situations. It is also similar to the relation derived by Matrosov et al. (2006) for a few light-to-moderate stratiform rainfall cases in Colorado that exhibited a bright band.

**8. Discussion and implications**

An important aspect of NBB rainfall is that it usually does not occur in isolation; rather it occurs interspersed in time and location with BB and convective rainfall as storms approach from the ocean (e.g., Fig. 2). The interspersed nature of NBB rain has physical and operational implications.

A physical implication of the interspersed nature of

NBB rain is that the microphysical processes that produce it often occur in superposition with BB rain. Hence BB rainfall over the coastal mountains is often microphysically enhanced compared to its nonorographic, upstream component. In the mountains, periods of shallow orographic rain are produced when the boundary layer upslope wind component is strong and water vapor content is high, as was shown quantitatively by White et al. (2003). But these predominantly NBB periods are usually punctuated intermittently with BB signatures when scattered deeper or higher clouds pass over and drop snowflakes into the orographic cloud. Then coalescence processes may accelerate rain rates beyond what either rain type would achieve alone. This was suggested by the “hybrid” rain category of White et al. (2003). As shown by Neiman et al. (2005), the BB periods become more dominant when fronts approach the mountains, bringing widespread deep clouds from the ocean. Then these BB periods are interrupted by occasional breaks in the deeper clouds that again reveal the underlying NBB rain. Studies of DSDs in BB rain sufficiently upstream of any underlying orographic clouds are needed to help clearly separate the two influences in these superposition situations.

Operational implications, mentioned in section 6, include the fact that two of the most commonly used NEXRAD  $Z-R$  equations result in large errors for estimating rain intensities and accumulations, when applied to NBB rain. Similarly, however, application of other  $Z-R$  relations, including the NBB equations derived in this study, to periods and regions of BB rainfall will also produce erroneous estimates. The current NEXRAD system is not capable of simultaneously applying different  $Z-R$  relations to different locations, such as coastal mountains and inland valleys, within individual scans.

Even if the use of multiple  $Z-R$  relations within individual sweeps becomes possible in the future, however, the more fundamental challenge will still be to identify and distinguish between different rain types and then apply the most appropriate  $Z-R$  relation to specific scan pixels. Section 7 showed that radar polarimetry may provide some help in this regard for BB/NBB rain. Networks of gap-filling radars, such as small, short-wavelength polarimetric scanning radars, or vertical profilers, which are considerably less expensive than S-PROF (now being designed at NOAA), might be very advantageous in some locales. These systems can also reduce the problems associated with NEXRAD’s inadequate low-altitude scan coverage that are especially prevalent in the western United States (e.g., Westrick et al. 1999). Meanwhile, this study

more clearly reveals the causes and magnitudes of one aspect of the problem on the West Coast, which is the significant difference between BB and NBB winter precipitation.

## 9. Summary and conclusions

Recent studies found that a large fraction of the winter rainfall in northern California and Oregon falls during periods when clouds overhead do not exhibit a melting-layer radar bright band (White et al. 2003; Neiman et al. 2005; Kingsmill et al. 2006). The studies called these periods “nonbrightband (NBB) rain” and deduced that microphysical characteristics of this precipitation differ in important ways from the more common brightband (BB) periods. Their conclusions were based on observations aloft using S-band profiling radars (S-PROF), but without the benefit of direct measurements of DSDs at the surface. The current investigation extends the earlier work by including new measurements using ground-based raindrop disdrometers to augment the S-PROF observations.

In the winter of 2003/04 disdrometers at two of the same locations (one on the coastline and one nearby in the coastal mountains) of the earlier studies in northern California recorded 365 h of rainfall and more than 14 million raindrops. As in the earlier studies, rainfall was objectively classified as BB, NBB, or convective, according to data from the collocated S-PROF.

The disdrometer data confirm microphysical inferences of the earlier work. The NBB periods contain larger concentrations of small raindrops ( $D < 1$  mm) and much smaller concentrations of large drops ( $D > 2$  mm), and greater total numbers of drops than BB periods. The disdrometer-measured DSD differences are consistent with the hypothesis that hydrometeor growth during BB periods is dominated by ice processes in a deep layer aloft, whereas growth in NBB periods is primarily the result of condensation and coalescence of water droplets in a relatively shallow layer near the surface. Comparisons of the S-PROF echo-top data with temperatures from radiosondes further support this concept. On average, the NBB echo tops were 3.2 km lower than those of BB cases, and extended only about 1 km above the 0°C level.

The conceptual model of Kingsmill et al. (2006) fits these new observations well (see their Fig. 17a). Deep storm clouds, associated with synoptic-scale forcing, commonly generate large snowflakes aloft, which produce a bright band and large raindrops as they fall through the 0°C level and melt. Relatively shallow orographic clouds, however, are populated by copious numbers of small raindrops produced mainly by condensational growth, but contain no large snowflakes, or

possibly no ice at all. These shallower clouds do not exhibit a bright band, except for times when a transient, colder cloud drops large snowflakes into them from above. When such natural seeding occurs, NBB rainfall is briefly transformed into BB rain.

Several DSD and rainfall parameters were computed from the observed drop spectra and examined for differences in the two types of nonconvective rainfall. The NBB periods exhibited mean values that were approximately the following percentages of their BB counterparts: 60% for mean-volume diameter, 68% for rainfall intensity, 187% for total number of drops, and 181% for slope of the spectra. Each of these differences is statistically significant at the 99% confidence level. The difference in mean values of liquid water content, however, was small and not significant.

DSDs for the BB periods are a close match to the Marshall–Palmer drop size distribution for the same average rain rates. The  $Z$ – $R$  relations ( $Z = aR^b$ ) computed from the DSDs observed by the disdrometers revealed contrasts that are also consistent with an earlier finding based on S-PROF and rain gauge data. Namely, the coefficient ( $a$ ) is much smaller for NBB than for BB periods of rain. For example, in the coastal mountains, the disdrometer-derived BB relation is  $Z = 168R^{1.58}$  and the NBB relation is  $Z = 44R^{1.91}$ . The nontropical convection and the stratiform/orographic relations commonly employed with NEXRAD radars underestimate accumulations in NBB situations by a factor of 2 or more when the relations are applied to observed DSD data. A NEXRAD relation recommended by the NWS for western U.S. cool-season rainfall approximates the NBB conditions better, but still underestimates accumulations substantially. The NBB results pertain to predominantly stratiform rain, and not to convective cells, in which the bright band is often also missing, but for other reasons.

Polarimetric radar parameters,  $Z_{DR}$ , and  $K_{DP}$ , were also computed from the observed DSDs. The NBB periods typically had lower  $Z_{DR}$  values than the BB periods. Thresholds of  $Z_{DR} \leq 0.2$  dB and  $Z_{DR} \geq 0.6$  dB may be useful for classifying areas of NBB and BB rainfall, respectively, using scanning polarimetric radars. Quantitative estimation of rainfall using  $K_{DP}$ – $R$  relations, however, only appears to be fruitful for BB rainfall observed with short-wavelength radars, such as X band. The very small  $K_{DP}$  signal is too noisy for reliable use in NBB rain at X band and in both NBB and BB rain at S-band wavelengths.

These findings have noteworthy implications for quantitative precipitation estimation by ground-based and spaceborne weather radars, at least for coastal orographic rainfall in the western United States and per-

haps elsewhere. The melting-layer bright band, which is characteristic of most midlatitude winter storms, is frequently absent in stratiform rain at these locations. Commonly employed  $Z$ - $R$  relations yield large underestimates of accumulation when applied to this situation, because the DSDs are markedly different from those that occur when a bright band is present. Furthermore, NBB rainfall should not be ignored. It contributes significantly to the total winter season rainfall at some locations, and includes moderately heavy and potentially flood-producing rain at times.

*Acknowledgments.* HMT is sponsored by NOAA. Coauthor Yuter's work was supported by National Science Foundation under Grant ATM 0121963. The disdrometer at CZD was provided courtesy of the University of Washington and coauthor Yuter, with engineering support by Dave Spencer. Jonathan Splitt of NOAA/ESRL contributed to preliminary aspects of the data analysis. David White and Scott Abbott of NOAA/ESRL maintained the disdrometer, S-PROF, and radiosonde systems in the field. The authors are grateful for all of these contributions to the study.

## REFERENCES

- Amitai, E., 2000: Systematic variation of observed radar reflectivity-rainfall rate relations in the tropics. *J. Appl. Meteor.*, **39**, 2198-2208.
- Blanchard, D. C., 1953: Raindrop size distribution in Hawaiian rain. *J. Meteor.*, **10**, 457-473.
- Brandes, E. A., and K. Ikeda, 2004: Freezing level estimation with polarimetric radar. *J. Appl. Meteor.*, **43**, 1541-1553.
- , G. Zhang, and J. Vivekanandan, 2004: Comparison of polarimetric radar drop size distribution retrieval algorithms. *J. Atmos. Oceanic Technol.*, **21**, 584-598.
- Bringi, V. N., and V. Chandrasekar, 2001: *Polarimetric Doppler Weather Radar: Principles and Applications*. Cambridge University Press, 636 pp.
- Campos, E., and I. Zawadzki, 2000: Instrumental uncertainties in  $Z$ - $R$  relations. *J. Appl. Meteor.*, **39**, 1088-1102.
- Ciach, G. J., and W. F. Krajewski, 1999: Radar-rain gauge comparisons under observational uncertainties. *J. Appl. Meteor.*, **38**, 1519-1525.
- Doelling, I. G., J. Joss, and J. Riedl, 1998: Systematic variations in  $Z$ - $R$  relationships from drop size distributions measured in Germany during seven years. *Atmos. Res.*, **47-48**, 635-649.
- Hagen, M., and S. E. Yuter, 2003: Relations between radar reflectivity, liquid-water content, and rainfall rate during MAP. *Quart. J. Roy. Meteor. Soc.*, **129**, 477-493.
- Joss, J., and A. Waldvogel, 1967: Ein spectrograph für niederschlagstrophen mit automatischer auswertung. *Pure Appl. Geophys.*, **68**, 240-246.
- Kingsmill, D. E., P. J. Neiman, F. M. Ralph, and A. B. White, 2006: Synoptic and topographic variability of northern California precipitation characteristics in landfalling winter storms observed during CALJET. *Mon. Wea. Rev.*, **134**, 2072-2094.
- Levin, Z., G. Feingold, S. Tzivion, and A. Waldvogel, 1991: The evolution of raindrop spectra: Comparisons between modeled and observed spectra along a mountain slope in Switzerland. *J. Appl. Meteor.*, **30**, 893-900.
- Marshall, J. S., and W. M. Palmer, 1948: The distribution of raindrops with size. *J. Meteor.*, **5**, 165-166.
- Matrosov, S. Y., D. E. Kingsmill, B. E. Martner, and F. M. Ralph, 2005: The utility of X-band polarimetric radar for quantitative estimates of rainfall. *J. Hydrometeorol.*, **6**, 248-262.
- , R. Cifelli, P. C. Kennedy, S. W. Nesbitt, S. A. Rutledge, V. N. Bringi, and B. E. Martner, 2006: A comparative study of rainfall retrievals based on specific differential phase shift at X- and S-band radar frequencies. *J. Atmos. Oceanic Technol.*, **23**, 952-963.
- , K. A. Clark, and D. E. Kingsmill, 2007: A polarimetric radar approach to identify rain, melting-layer, and snow regions for applying corrections to vertical profiles of reflectivity. *J. Appl. Meteor. Climatol.*, **46**, 154-166.
- Neiman, P. J., G. A. Wick, F. M. Ralph, B. E. Martner, A. B. White, and D. E. Kingsmill, 2005: Wintertime nonbrightband rain in California and Oregon during CALJET and PACJET: Geographic, interannual, and synoptic variability. *Mon. Wea. Rev.*, **133**, 1199-1223.
- Sheppard, B. E., and P. I. Joe, 1994: Comparison of raindrop size distribution measurements by a Joss-Waldvogel disdrometer, a PMS 2DG spectrometer, and a POSS Doppler radar. *J. Atmos. Oceanic Technol.*, **11**, 874-887.
- Smith, P. J., and J. Joss, 1997: Use of fixed exponent in adjustable  $Z$ - $R$  relationships. Preprints, *20th Conf. on Radar Meteorology*, Austin, TX, Amer. Meteor. Soc., 254-255.
- Steiner, M., and J. A. Smith, 2000: Reflectivity, rain rate, and kinetic energy flux relationships based on raindrop spectra. *J. Appl. Meteor.*, **39**, 1923-1940.
- , —, and R. Uijlenhoet, 2004: A microphysical interpretation of radar reflectivity-rain rate relationships. *J. Atmos. Sci.*, **61**, 1114-1131.
- Testud, J., S. Oury, R. A. Black, P. Amayenc, and X. Dou, 2001: The concept of "normalized" distribution to describe raindrop spectra: A tool for cloud physics and cloud remote sensing. *J. Appl. Meteor.*, **40**, 1118-1140.
- Tokay, A., A. Kruger, and W. F. Krajewski, 2001: Comparison of drop size distribution measurements by impact and optical disdrometers. *J. Appl. Meteor.*, **40**, 2083-2097.
- Waldvogel, A., 1974: The  $N_0$  jump of raindrop spectra. *J. Atmos. Sci.*, **31**, 1067-1078.
- Westrick, K. J., C. F. Moss, and B. A. Colle, 1999: The limitations of the WSR-88D radar network for quantitative precipitation measurement over coastal western United States. *Bull. Amer. Meteor. Soc.*, **80**, 2289-2298.
- White, A. B., D. J. Gottas, E. T. Strem, F. M. Ralph, and P. J. Neiman, 2002: An automated brightband height detection algorithm for use with Doppler radar spectral moments. *J. Atmos. Oceanic Technol.*, **19**, 687-697.
- , P. J. Neiman, F. M. Ralph, D. E. Kingsmill, and P. O. G. Persson, 2003: Coastal orographic rainfall processes observed by radar during the California Land-Falling Jets Experiment. *J. Hydrometeorol.*, **4**, 264-282.
- Yuter, S. E., and R. A. Houze Jr., 1995: Three-dimensional kinematic and microphysical evolution of Florida cumulonimbus. Part II: Frequency distributions of vertical velocity, reflectivity, and differential reflectivity. *Mon. Wea. Rev.*, **123**, 1941-1963.
- Zrnić, D. S., and A. V. Ryzhkov, 1996: Advantages of rain measurement using specific differential phase. *J. Atmos. Oceanic Technol.*, **13**, 454-464.

Copyright of *Journal of Hydrometeorology* is the property of *American Meteorological Society* and its content may not be copied or emailed to multiple sites or posted to a listserv without the copyright holder's express written permission. However, users may print, download, or email articles for individual use.